Cores for Concern: How well do seafloor deposits represent the flows that created them?

William Symons, University of Southampton, UK

Mentors: Dr. Charlie Paull, Dr. Esther Sumner

Summer 2014

Keywords: Monterey Canyon, turbidity current, grain size analysis

ABSTRACT

Submarine canyons and the sedimentary processes operating within them are very poorly understood as a result of their relative inaccessibility and therefore the difficulty of making direct observations. Much of our understanding of the dynamics of sediment-laden flows in submarine canyons results from making inferences from the deposits that they leave behind in the geological record. This project tests how well such deposits in submarine canyons represent the flows that created them by comparing the sedimentary record on the floor and walls of Monterey canyon with the sediments collected in sediment traps during flow events. The project makes use of transects of push cores and vibracores collected from the canyon axis and canyon walls at altitudes from 0 to 70 m above the thalweg. The cores were collected by MBARI in 2014 in the vicinity of sediment traps deployed in 2002 by the US Geological Survey. Laser particle size analysis was used to analyse the grain-sizes present in the and was directly compared to deposits from the sediment traps, previously analysed using the same techniques. Preliminary results suggest that using deposits to reconstruct flows may not be as robust as previously thought, with sand distribution on the canyon walls not always accurately representing what was captured in the sediment traps. Three hypotheses are discussed to suggest reasons for this unexpected sand distribution: (1) A flow evolving down slope, (2) a flow superelevating, and (3) a flow being in a non-depositional and non-erosive state whereby it bypasses the system.

1.0 INTRODUCTION

Submarine canyons (canyons herein) are among the most dramatic geomorphic features on continental margins (Shepard 1981; Twichell & Roberts 1982). The accumulation of vast amounts of terrestrial material downstream from canyons in deep-sea fans (Paull et al. 2013) suggests that canyons are preferential conduits for sediment transport from the shelf to the deep sea (Puig et al. 2003). The shapes of canyons typically reflect the processes that transport sediment through them, deposit sediment within them, and erode into the underlying bedrock of the canyon (Paull et al. 2011). That said, unlike our knowledge of comparable environments in the terrestrial realm, our

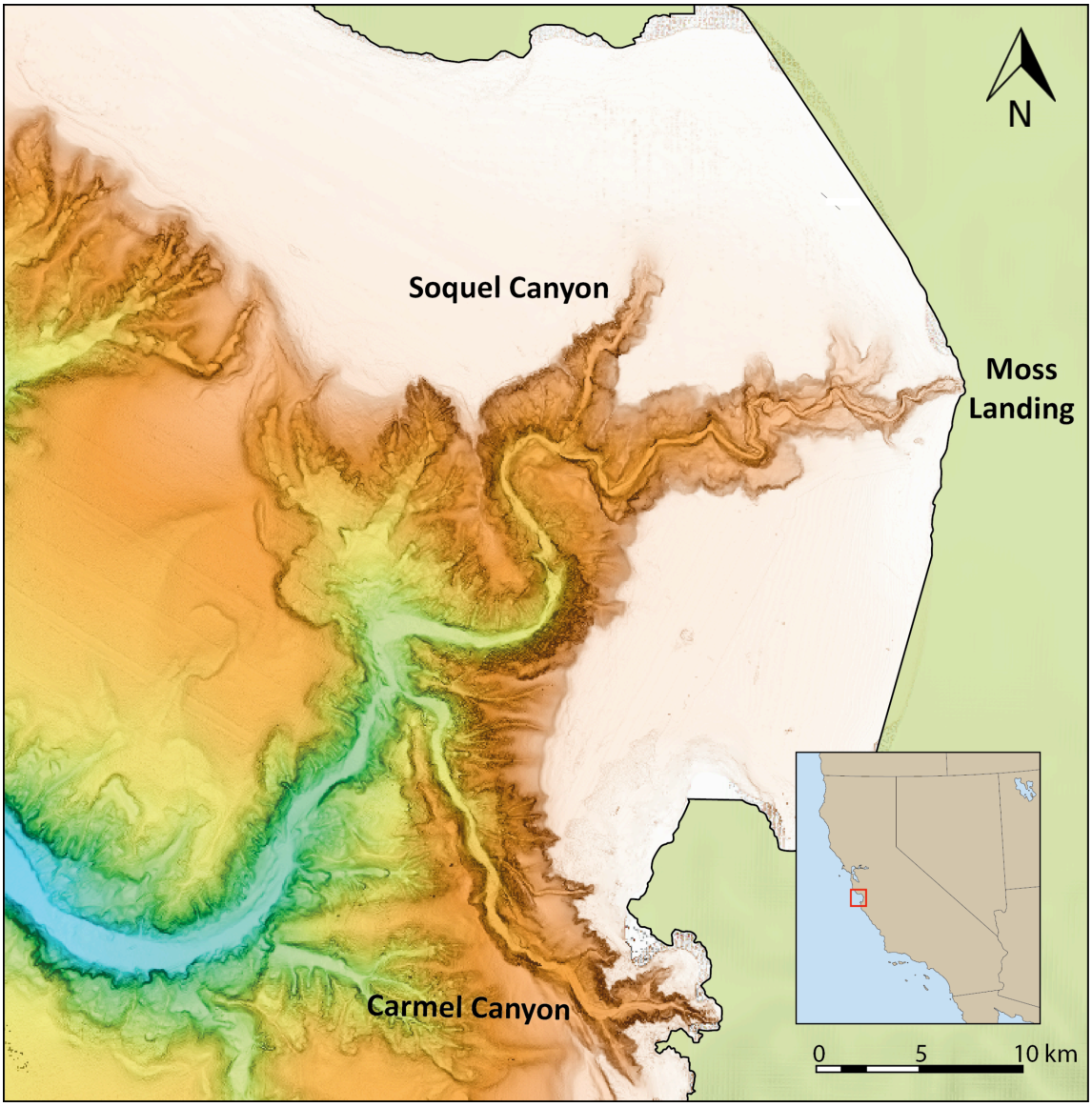

Figure 1: Map showing bathymetry of Monterey Bay and Monterey Canyon. Inset map shows location of Monterey Bay with respect to California.

understanding of the exact processes of sediment transport within canyons is limited and the subject of on-going investigation (Puig et al. 2014). The main limiting factor in our understanding is technology (Paull et al. 2005) because sampling, monitoring and imaging such a complex, heterogeneous and inaccessible environments is challenging.

Monterey Canyon is a distinct submarine geomorphic feature in Monterey Bay, California, and is the focus of this study (figure 1). The canyon head is only ~100 m from the shore (Talling et al. 2013) and the canyon can be traced for more than 400 km seaward to water depths >4000 m (Paull et al. 2011). Two main tributaries are present; Soquel Canyon and Carmel Canyon, which join Monterey Canyon at water depths of 980 m and 1970 m respectively. Monterey Canyon is active as its head is currently connected to the shore, with about 400,000 m^3 of sand descending through the canyon each year (Paull et al. 2003), with known sediment transport events occurring with a sub-annual frequency down to 1850 m water depth (Xu et al. 2004; Xu et al. 2014; Talling et al. 2013).

The existing paradigm is that turbidity currents and other gravity flows are responsible for large movements of sediment through canyons, including Monterey Canyon (Twichell & Roberts 1982; Puig et al. 2014; Paull et al. 2003; Xu et al. 2014), and are arguably the most important flow processes for moving sediment across the planet (Talling et al. 2012). Turbidity currents are a type of sediment density flow whereby the flow is fully turbulent and sediment is supported primarily by fluid turbulence, although this may be suppressed within near bed layers (Talling et al. 2013).

These flows are important to understand as they can travel very fast, up to velocities of at least 19 m/s, and break important sea floor infrastructure such as networks of seafloor cables (Piper et al. 1999; Hsu et al. 2008; Cattaneo et al. 2012). Damaging these cables proves very costly as these cables transfer more than 95% of transoceanic data (Carter et al. 2009; Talling et al. 2013). Similarly, these currents are also very damaging to industrial seafloor infrastructure, such as the costly setups used for recovering oil and gas (Barley 1999). Turbidity currents and subsequent deposits play a vital roll in burial of organic carbon and the therefore in the global carbon cycle (Galy et al. 2007; Talling et al. 2013). Additionally, earthquakes are thought to act as a causative mechanism for large slope failures and therefore turbidity currents. The resultant

turbidites may therefore provide a long-term record of major earthquakes (Goldfinger et al. 2007), although the record may be incomplete (Sumner et al. 2013). Is it therefore clear that developing our understanding of how sediment is transported is vital for hazard prediction and preparation, and effective oil and gas recovery.

A number of mechanisms for the triggering of turbidity currents have been proposed. Firstly, earthquakes can cause widespread seabed slumping and therefore en masse sediment movement which results in downslope movement, such as the Grand Banks earthquake (Piper et al. 1999). Sediment slumping and slope failures can also result from the rapid addition of sediment to the head of a canyon from human influence, such as causing instability of established sediment (Piper & Savoye 1993). Strong wave action can also cause rapid deposition of sediment into a canyon head and destabilise slopes by cyclic loading (Paull et al. 2003). Finally, the rapid deposition of sediment onto canyon head deposits and shelf sediment can occur from the plunging of hyperpycnal river floodwater as in the case of the Zaire canyon (Khripounoff et al. 2003).

Arguably the most important measurement for characterising a turbidity current is the vertical profile of sediment concentration and grain size, which is currently collected from light backscatter or Acoustic Doppler Current Profiler (ADCP) backscatter data (Talling et al. 2013). That said, to date there is data from only four locations in canyons or delta fronts/channels (Xu et al. 2004; Xu 2010; Xu 2011; Hughes Clarke et al. 2012; Liu et al. 2012; Xu et al. 2014), highlighting the difficulties in monitoring these currents. The lack of direct measurements of turbidity currents means that a key step in attempting to understand flow processes is by studying turbidity current deposits. Interpretations based on the characteristics of the deposit, as well as the channel morphology can provide insight into the possible structure and evolution of flows. Previous attempts have been made to model currents based on channel morphology, numerical modelling and sediments (cores), particularly the Amazon Channel (Pirmez & Imran 2003). Many parameters such as flow density, water entrainment and acceleration are poorly constrained and were estimated, with other parameters such as flow velocity being a function of these estimated parameters (Pirmez & Imran 2003). In the case of the Amazon Channel, sediment grain size, along with the above parameters were used to estimate cross-channel flow stratification. It is known that the currents that pass through

the Amazon Channel are a mix of sand and mud (sand:mud ratio of 5-10%), yet only mud is found on the levees and overbank deposits, despite the thickness of the flow exceeding the relief of the channel. The lack of sand in the overbank therefore suggests the vertical stratification of grain sizes within the flow, with sand confined to the lower 20-30 m of the flow (Pirmez & Imran 2003). A similar grain-size approach was adopted by Stevenson et al (2013). Along with chronostratigraphic and geochemical approaches, turbidites were correlated between basins and through channels via a suite of cores. Additionally, sedimentary structures were studied in detail to better assess the nature of the flows. The dominance of ripple cross-laminated sands indicated that the parent flow was relatively dilute and depositing incrementally via tractional reworking (Stevenson et al. 2013). The vertical grading of the deposits also allowed for determination of the longitudinal structure of the base of the flow. Stevenson et al. (2013) were able to correlate individual deposits across two basins, yet there were no deposits in the channel system connecting the two basins. This led them to deduce that these turbidity currents reached a state whereby they were neither erosive nor depositional but bypassed their sediment through the system, leaving no trace.

As a result of difficulties in directly monitoring turbidity currents, it is clear that the main way we have to reconstruct flows is from their deposits. This said, there has never been a data set that can test the viability of using deposits to reconstruct flows. In this study we present a suite of 35 cores, from three transects across Monterey Canyon and we compare this to published data from sediment traps from two of the three locations (Xu et al. 2014). This is the first study that can directly compare seafloor deposits from turbidity currents to samples collected directly from the flow. This study therefore aims to:

(1) Describe and understand the facies present in Monterey canyon from a continuous range of heights from the thalweg up the canyon walls.

(2) Determine whether grain sizes that are present at a given height within a flow (70 MAB) are found at the same level on the canyon wall, and if they are not then at what level are they found?

(3) To use the above information to understand how well we can infer flow characteristics (e.g. flow thickness) from deposits

2.0 MATERIALS AND METHODS

2.1 ROV CORING

On 16, 18 and 19 April 2014 the ROV *Doc Ricketts* collected 35 vertical vibracores along three cross-sectional transects within Monterey Canyon between 754 and 1282 m water depth (figure 2). Transect 1 (Tr1, or 'proximal transect') consists of 12 vibracores collected during dives DR585 and DR586 in water depths 754 to 830 m on the north wall of the canyon. Transect 2 (Tr2, or 'confluence transect') comprises 11 vibracores collected during dives DR589 and DR590 in water depths of 953 to 1019 m on the southern wall of the canyon, slightly downstream of the confluence of Soquel Canyon and Monterey canyon. The final transect (Tr3, or 'distal transect') was collected during dives DR591 and DR592 and consists of 12 vibracores, collected form the eastern/southern wall in 1209 to 1282 m of water. The shallowest vibracore from each transect (the core highest on the canyon wall) was taken at approximately the same level as the sediment trap (70 MAB) deployed by Xu et al (2014).

The ROV *Doc Ricketts* coring system is capable of collecting up to six 1.8 m long and 7.65 cm diameter cores in aluminium tubes (Paull et al. 2013). The benefit of using an ROV coring system is the unrivalled accuracy for coring location, especially within such a heterogeneous environment as a submarine canyon. The vibracores were logged for p-wave velocity and ϒ-attenuation with a GEOTEK multisensory core logger. The cores were then longitudinally split and photographed with a GEOTEK digital line-scanning camera, and archived at the U.S. Geological Survey (USGS) in Menlo Park, California.

The ROV manipulator arm has the ability of collecting push cores up to 25 cm in length in soft to semi-consolidated sediment (Paull et al. 2013). A total of 108 push cores

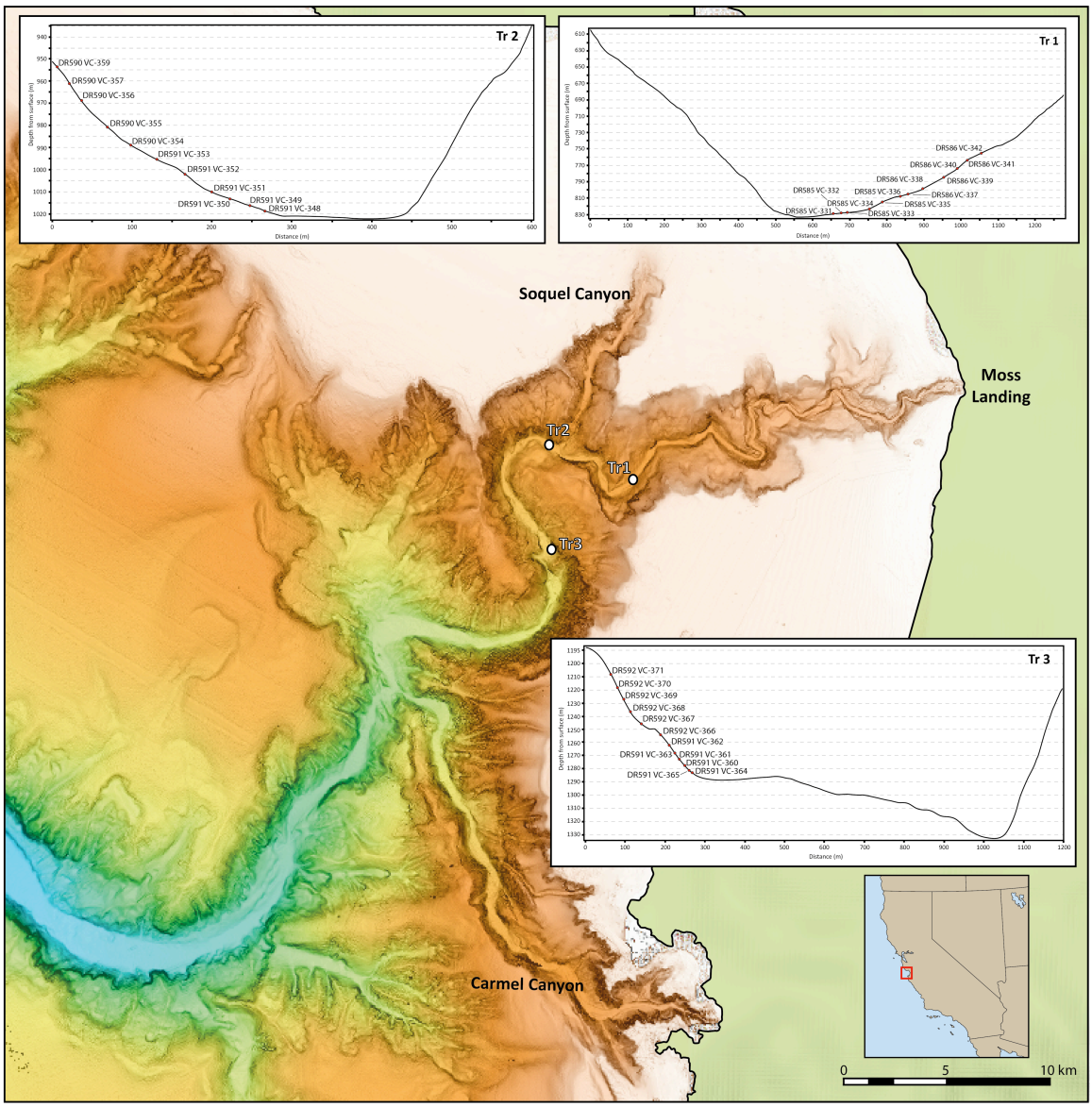

Figure 2: Bathymetry of Monterey Bay and Monterey Canyon out to 2300 m water depth. Included are the cross-sectional views of the three transect locations (Tr1, Tr2 and Tr3) looking down canyon. Each has the location of the vibracores added. Inset map shows location of Monterey Bay with respect to California.

were collected: three push cores were collected from every vibracore location and an additional core was collected at three locations. All of the push cores were processes onboard: one push core was extruded from its tube, split lengthways and described; the remaining push cores were cut into 1 cm thick vertical slices and archived for paleo- and grain-size analysis.

2.2 FACIES DETERMINATION

Visual core logging was undertaken on all vibracores, paying particular attention to grain-size changes and colour, especially within the mud horizons. Any sedimentary structures were noted and graphically represented for process interpretation.

2.3 GRAIN SIZE ANALYSIS

Grain-size analysis was conducted on a sub-sample of the 1 cm push core slices. The push cores (as opposed to vibracores) were chosen for this initial analysis as it is probable that these deposits are of similar age to the sediments deposited within Xu et al's (2014) sediment traps. Additionally, the push cores were already available for analysis without causing damage to the vibracores, thus preserving them for future analysis. Every other push core from each transect was analysed and this always included the highest altitude core that correspond in height with Xu et al.'s (2014) sediment trap. Two sample swere taken from each push core (i) the slice with the coarsest material and (ii) the slice that visually appeared to contain the finest sediment.

To ensure that the results of this study were directly comparable to those within Xu et al (2014), grain-size analysis was undertaken on the same Beckman Coulter LS230 laser diffraction particle size analyser, located at the USGS field office in Santa Cruz, California. Sample preparation also followed the same process used by Xu et al (2014) and is outlined below.

Approximately 20 g of sediment was placed into individual 1000 mL beakers where 10 mL of 35% hydrogen peroxide (H_2O_2) was added along with sufficient distilled (DI) water to make a 300 mL solution. This solution was left overnight in order to remove organics and begin the process of sample dispersion. The following day, the samples were placed onto a hotplate set at 250-300 °C for 2-3 hours, or until the solution was concentrated to 200 mL: this ensures that any hydrogen peroxide was removed. Following this, each beaker was placed into an ultrasonic bath for 10 minutes to continue the disaggregation of fine mud particles.

The removal of soluble salts required two runs in a centrifuge. Samples were transferred into 250 mL centrifuge bottles. The bottles were weighed and in pairs, topped up with DI water to within 0.1 g of each other. Each bottle within a pair was placed

opposite each other within the centrifuge to ensure it was correctly balanced. Samples were centrifuged initially for 1 hour at 1700 rpm. After this initial run, samples were removed and the supernate removed without losing sample before samples were re-weighed while adding DI water for a second 30 minute run at 1700 rpm. Following this, each sample had 5 mL of sodiumhexametaphosphate (calgon) added to disperse negatively charged clay particles. To ensure the weight of the calgon was accounted for, three aluminium trays were weighed before 5 mL of calgon was added and left to dry overnight in the oven.

Wet sieving was used to separate the sand and silt (2000-63 μm) fraction from the fines and mud fraction (<63 μm). Samples were washed: sand a silt sized grains were trappedin the sieve stack. Sand and silt were washed from the sieve and transferred into a crucible and then dried in an 80-110 °C oven overnight. Each graduated cylinder was topped up with DI water to 1000 mL and left overnight.

The weight of each sample (both the dried sand and silt weight and the fines) was determined. The dry sand and silt were weighed and recorded. The dried weight of 20 mL of the fines solution was determined by drying the solution in an oven overnight and deducting the known weight of the calgon.

The Coulter counter was operated using the same protocol and parameters as described in Xu et al (2014). Approximately 1-2 g of sample was needed, with finer–grained samples requiring less sediment to achieve the correct obscuration. If the sample exceeded this 1-2 g guide, then it was split using a sand splitter before being added to the coulter chamber. Most samples were run using an obscuration of ~30%. It was necessary to run some samples with an obscuration as low as 4%. For the fine samples, the sample was transferred to a beaker and agitated using a motorised stirrer in order to achieve a homogeneous suspension. After two minutes of stirring a sample was taken using a pipette and added into the Coulter chamber. Each sample was passed through the counter three times, although the first run was discarded, because air bubbles were often present. The second and third runs were compared and if similar, then results were averaged. Between each run, the system was flushed to ensure no residual grains from the previous sample remained in the system. The coarse and fine samples, from a single grain-size

sample (i.e. one push core slice), were combined using the bespoke USGS software, pc SDSZ, at the end of each run.

3.0 RESULTS

3.1 FACIES DESCRIPTIONS

Four types of facies were identified in vibracores (figure 3):

(1) **Facies 1 – *Silt and mud***. Very little size variation, colour varies from light grey to (dark) brown. Occasional organic and very fine lithic bands and diffuse patches present. This was the dominant facies (by total thickness) in cores from 21.92 m altitude (relative to the deepest core in a transect) in transect 1, 7.93 m in transect 2, and 30 m in transect 3.

(2) **Facies 2** – ***Sand beds with clasts of cohesive mud.*** Sand is dominant with internal mud clasts and varying angles. Overall appearance is disturbed. This facies was present in the confluence and distal transects from areas around or on terraces at 29 m altitude in transect 2 and 20 m altitude in transect 3. Key example is DR589 VC-352, 4-28 cm (figure 3). Two clear sub-facies can be deduced based primarily on colour. Darker mud, typically dark grey and brown, is the most prevalent. A paler mud is consistently found above normally graded sand.

(3) **Facies 3** – ***Normally graded sands.*** Beds range in thickness from 0.5 to 10 cm but typically 1-2 cm. Bases can be diffuse but are typically erosive, defined by sharp, irregular contacts and occasional inclusion within underlying material. Grading is normal but hard to determine in thinner beds. This facies is found in all cores and at the full range of altitudes. Key example is DR589 VC-352, 64-65 cm (figure 3).

(4) **Facies 4** – ***Chaotic sands.*** Deposits display a wide variety of grain sizes in irregular and inconsistent grading patterns if present but typically ungraded. This is the coarsest grained facies and occurs within the lowest altitude cores within a given transect. The confluence and distal transects have this facies restricted to

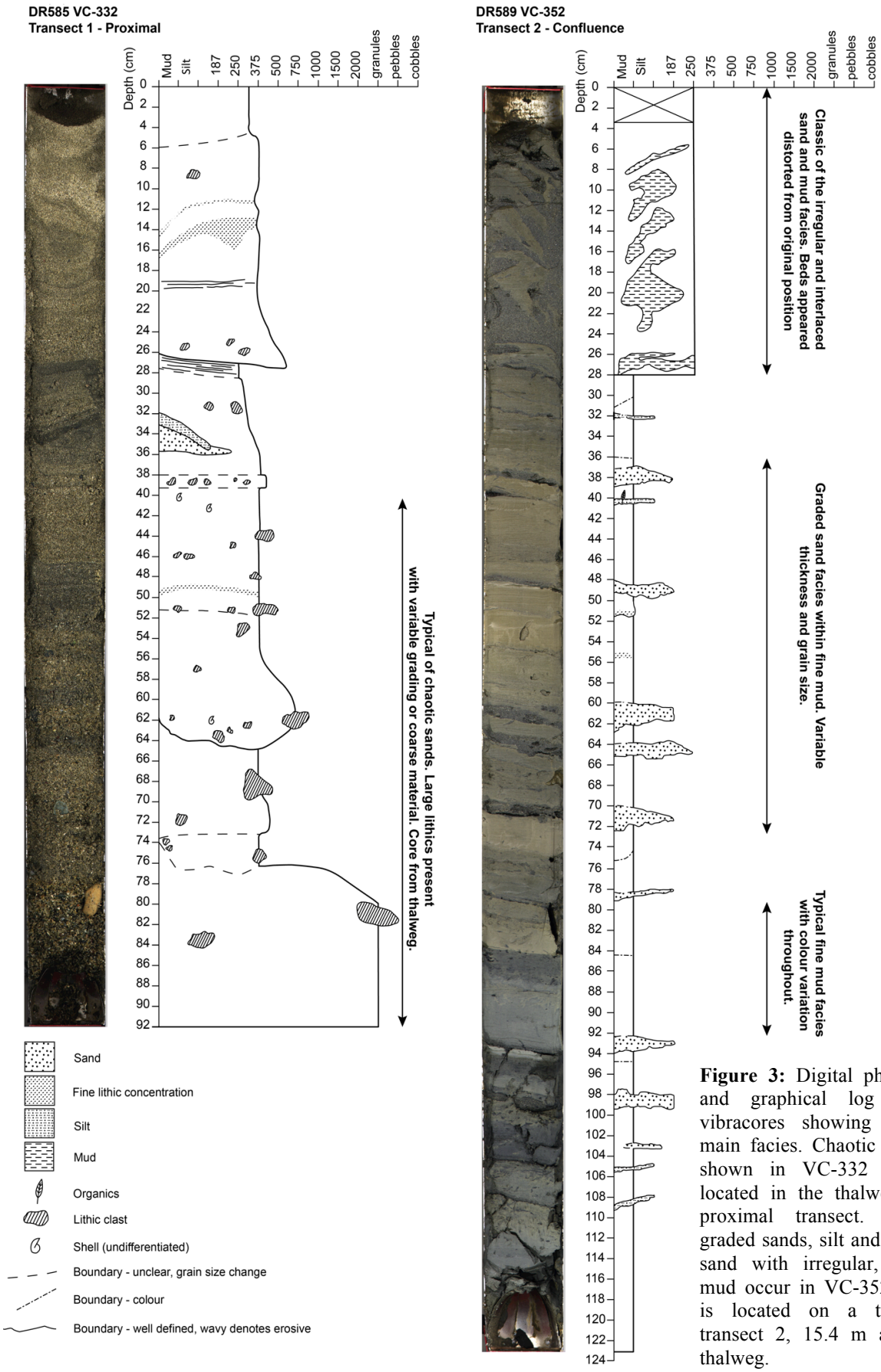

Figure 3: Digital photographs and graphical log of two vibracores showing the four main facies. Chaotic sands are shown in VC-332 which is located in the thalweg of the proximal transect. Normally graded sands, silt and mud, and sand with irregular, cohesive mud occur in VC-352m which is located on a terrace in transect 2, 15.4 m above the thalweg.

the lowest 2 m but the proximal transect sees chaotic sands as high as 7 m. large lithic clasts provide initial identification. Key example is DR 585 VC-332, 52-92 (figure 3).

The composition of sands is similar between cores. Quartz is the primary component of the sand and is characteristically sub- to well-rounded and of high sphericity. Undefined lithics are present and are typically sub-angular with a variable sphericity. The lithics are usually of a smaller size than the quartz grains. Biotite is often present both within the sand and dispersed throughout mud sequences (finer). Biotite in the sand is usually larger than the quartz and lithic grains; it is a minor component.

The heterogeneous nature of the cores means that not all facies are represented in a single core and there is a high level of variation even between adjacent cores. Despite this, characteristics based on facies and features of the cores are apparent. Bioturbation is prevalent in both the confluence and distal transects but is not apparent in the proximal transect. Bioturbation is typically isolated to facies 1 and occurs above 30 m altitude. Bioturbation is usually recognised from patchy mud discolouration and small concentrations of coarser material within the mud. Burrows were also present where depressions of a distinct horizon into a 'U' shape were in filled with typically coarser material than the deformed layer. In addition, the presence of discontinuous sand horizons that were once clearly continuous is attributed to bioturbation: these are represented on the graphical log by a gap in the sand horizon.

Dewatering structures were also present in some cores. A good example of dewatering is in DR589 VC-349 where the dewatering structure occurs within a massive sand. Dewatering structures were recognised by vertical to sub-vertical streaks of darker material than the surrounding sand. Finer material, often with a mud component, has replaced the sand where fluid has passed through. The structures are discontinuous and are at a maximum, 8cm in length, although typically no more than 4 cm, with widths less than 1 cm.

Colour variations are present within facies 1. Fine, variably angular black lithic grains are often found in fine layers within mud sequences. This often results in slight grain size increases when logging, such as at 51 cm in DR589 VC-352 (figure 3).

Additionally, fine lithics can be found as discrete horizons without varying grain size (e.g. 50 cm in DR585 VC-332) and in some cases, creating fine scale laminations (e.g. 26-28 cm, DR585 VC-332). Colour variations in facies 1 also occur without the influence of lithics. Natural colour changes, often in irregular, wavy boundaries occur within the middle of a facies 1 sequence. The colour change occasionally defines the change to a more cohesive mud. Lighter muds are often associated with facies 3 where a small deposit of lighter mud sits above a facies 3 horizon (e.g. DR589 VC-352, 36 cm).

3.2 SAND DISTRIBUTION WITHIN TRANSECTS

The amount of clean sand (i.e. non muddy horizons >63μm) within each vibracore was measured from the graphical logs. This enabled the calculation of sand: mud (i.e. net: gross (N/G)) for each core. Only beds that crosscut the entire width of the core or showed evidence of having originally crosscut the width of the core (e.g. bioturbated sand layers) were counted.

In general, the proportion of sand progressively decreases with increasing altitude above the thalweg, most noticeably in the proximal and distal transects, albeit there is more scatter in the distal transect (figure 4). In contrast, at the confluence, sand content does not progressively decrease but fluctuates with altitude above the thalweg (figure 4).

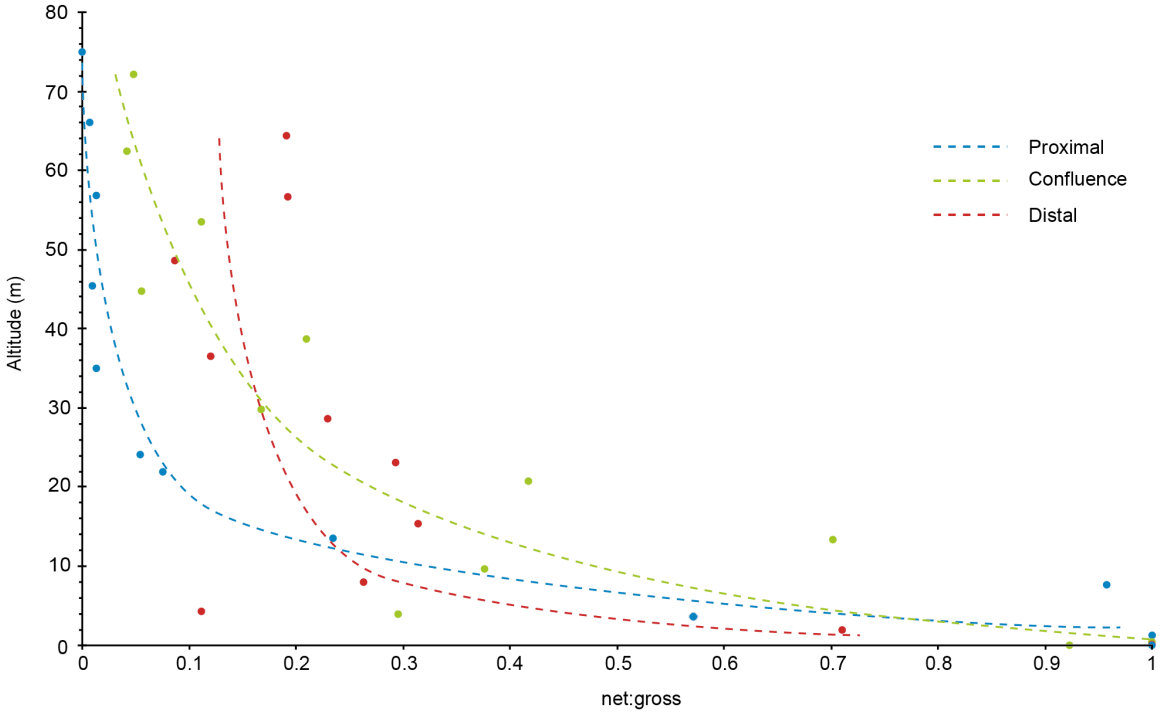

Figure 4: Proportion of sand:mud (net to gross) plotted against altitude above thalweg. Blue points are cores from transect 1 (proximal), red is from transect 2 (confluence), and green points are from transect 3 (distal).

Sand was present in all but one core (DR586 VC-342), found in the proximal transect. The amounts of sand within the proximal transect decreases sharply, from 100% in cores within the thalweg to ≤10% sand above 20 m altitude. The sand content progressively decreases to 0% at 75 m altitude. Similarly, the distal transect has a sharp drop in sand content below 10 m altitude. Contrastingly however, the sand content increases sharply again from 10-15 m altitude before progressively decreasing, with minor fluctuations at ~40 and 55 m altitude, to a minimum of ~4% sand at 62 m altitude. The confluence transect shows a sharp decrease of sand content from 100% to ~10% within the first 5 m of altitude. Above this attitude the sand content fluctuates far greater than the proximal and distal transects. Sand content varies between 31% at 15.5 m altitude and 8% at 48 m altitude, before reaching a sand content of 19% at 65 m altitude. The confluence transect has the highest sand content within the core at the greatest altitude.

The push cores represent the most recent sediments deposited in the canyon, whereas the vibracores extend the record further back in time. We are interested in understanding how representative the push cores are of the longer record of deposition. To achieve this we plotted the maximum grain size in each core versus altitude above the thalweg (figure 5). Note that grain size was determined using hand lens and grain-size comparator visually for the vibracores and by laser particle size analysis using the Coulter counter for the push cores. The vibracores show a

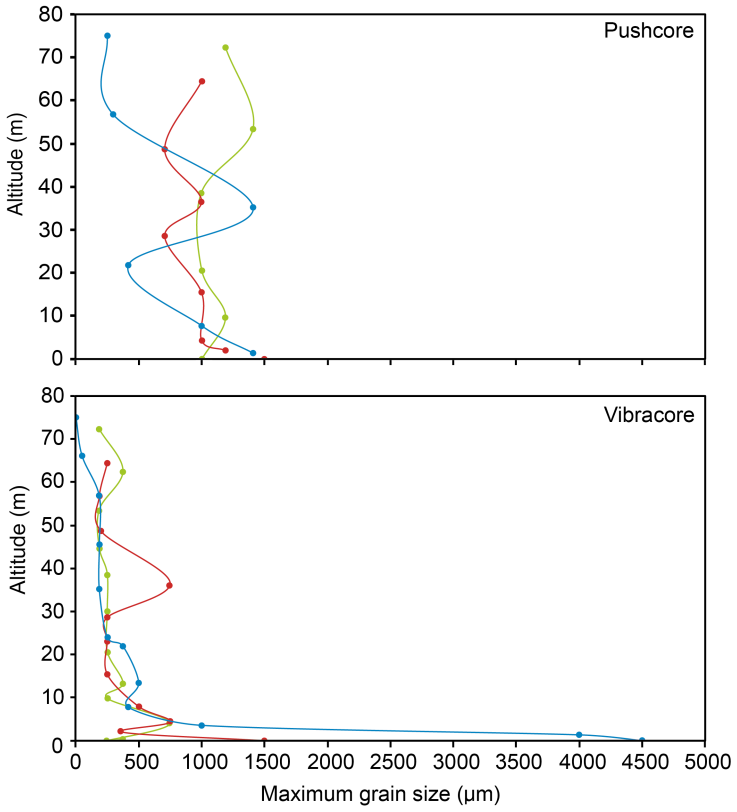

Figure 5: Graphs showing maximum grain size versus altitude above thalweg. A) Grain-size trends based on measurements from push cores using the Coulter counter B) Grain-size trends determined from vibracores using a hand lens and grain size comparator. For both, blue is transect 1, red is transect 2, and green is transect 3.

fining up of maximum grain size within the first 10 m from the thalweg (figure 5). The fining up of maximum grain size continues for the most proximal transect of vibracores. Above 10 m altitude for the confluence and distal transects there is minimal, if any, fining of the maximum grain size. Overall, there is a lot of variability/fluctuation in grain size for all transects. The push cores do not show a fining up of grain size within the first 10 m and is attributed to the fact that the push cores associated with the deepest thalweg deposits were not sampled. The push cores show greater variability in maximum grain sizes for a given transect. Additionally, the push cores show an overall coarser maximum grain size than the vibracores but this is attributed to the difference in grain size determination between the push cores and vibracores. In comparison with the vibracore dataset, the push cores do not show fining up of the deposits within the confluence and distal transects. Similarly to the vibracores, the proximal transect for the push core data does show a fining up from the deepest to shallowest deposits, although with much greater variability. Both datasets show on sharp increase in grain size at ~40 m altitude in the confluence transect (red). Interestingly, the same grain size jump is shown in the proximal transect but only for the push core data.

3.3 GRAIN SIZE

The grain-size data from each sampled push core are shown in figures 6-8 along with an underlay of Xu et al's (2014) sediment trap data from the same location (if available) from 70 MAB.

Data presented at the proximal location by Xu et al (2014) show a sharp peak centred around ~250 μm. A broader peak extending from 0.35 μm to ~210 μm represents the finer material within the sediment trap (figure 6). Push core 60 at 75 m altitude is closest in altitude to the sediment trap of Xu et al (2014). The grain sizing produces trends akin to the finer sample of Xu et al (2014). A broad peak is seen for both our fine sample (blue) and coarse sample (red) from 0.35 μm to 250 μm for both samples (figure 6). The amount of grains at the coarsest boundary is however extremely low (<0.1%) and is not considered of significant levels. Grains of 125 μm constitute 1.2% of the coarsest sample and should therefore be the coarsest upper limit for this broad peak, highlighting that the same sized sand is not seen at the side of the canyon as is seen in the sediment

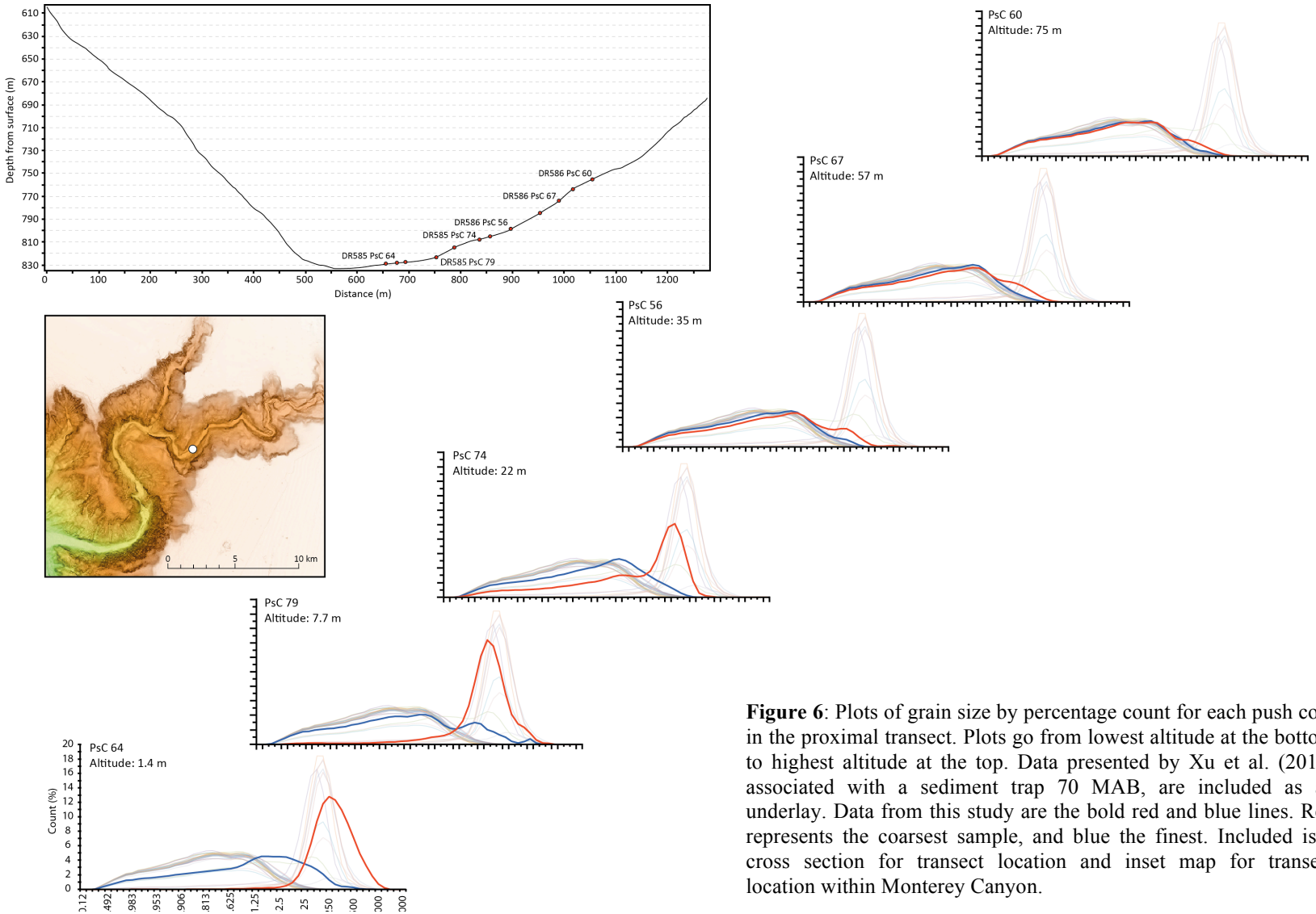

Figure 6: Plots of grain size by percentage count for each push core in the proximal transect. Plots go from lowest altitude at the bottom to highest altitude at the top. Data presented by Xu et al. (2014) associated with a sediment trap 70 MAB, are included as an underlay. Data from this study are the bold red and blue lines. Red represents the coarsest sample, and blue the finest. Included is a cross section for transect location and inset map for transect location within Monterey Canyon.

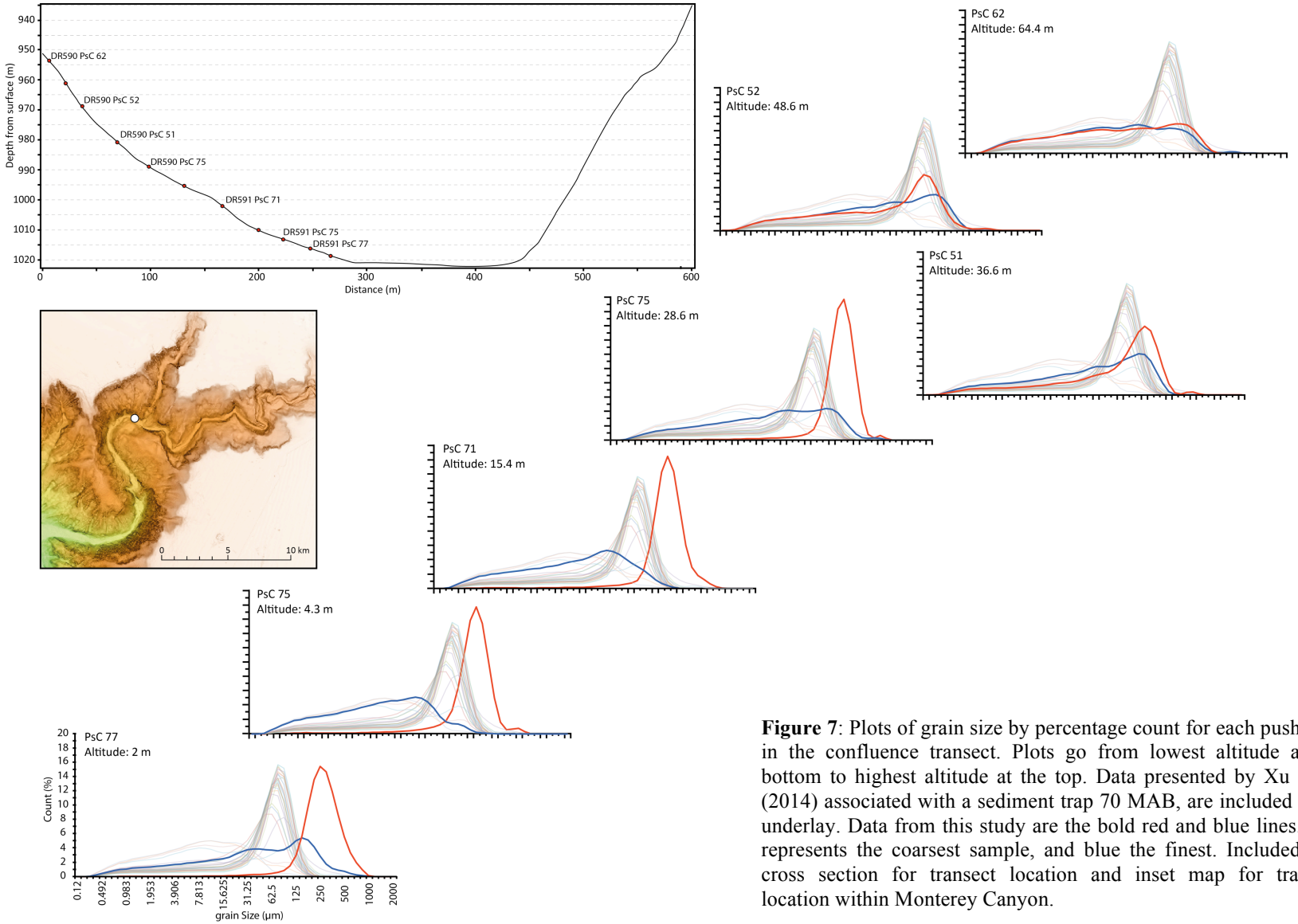

Figure 7: Plots of grain size by percentage count for each push core in the confluence transect. Plots go from lowest altitude at the bottom to highest altitude at the top. Data presented by Xu et al. (2014) associated with a sediment trap 70 MAB, are included as an underlay. Data from this study are the bold red and blue lines. Red represents the coarsest sample, and blue the finest. Included is a cross section for transect location and inset map for transect location within Monterey Canyon.

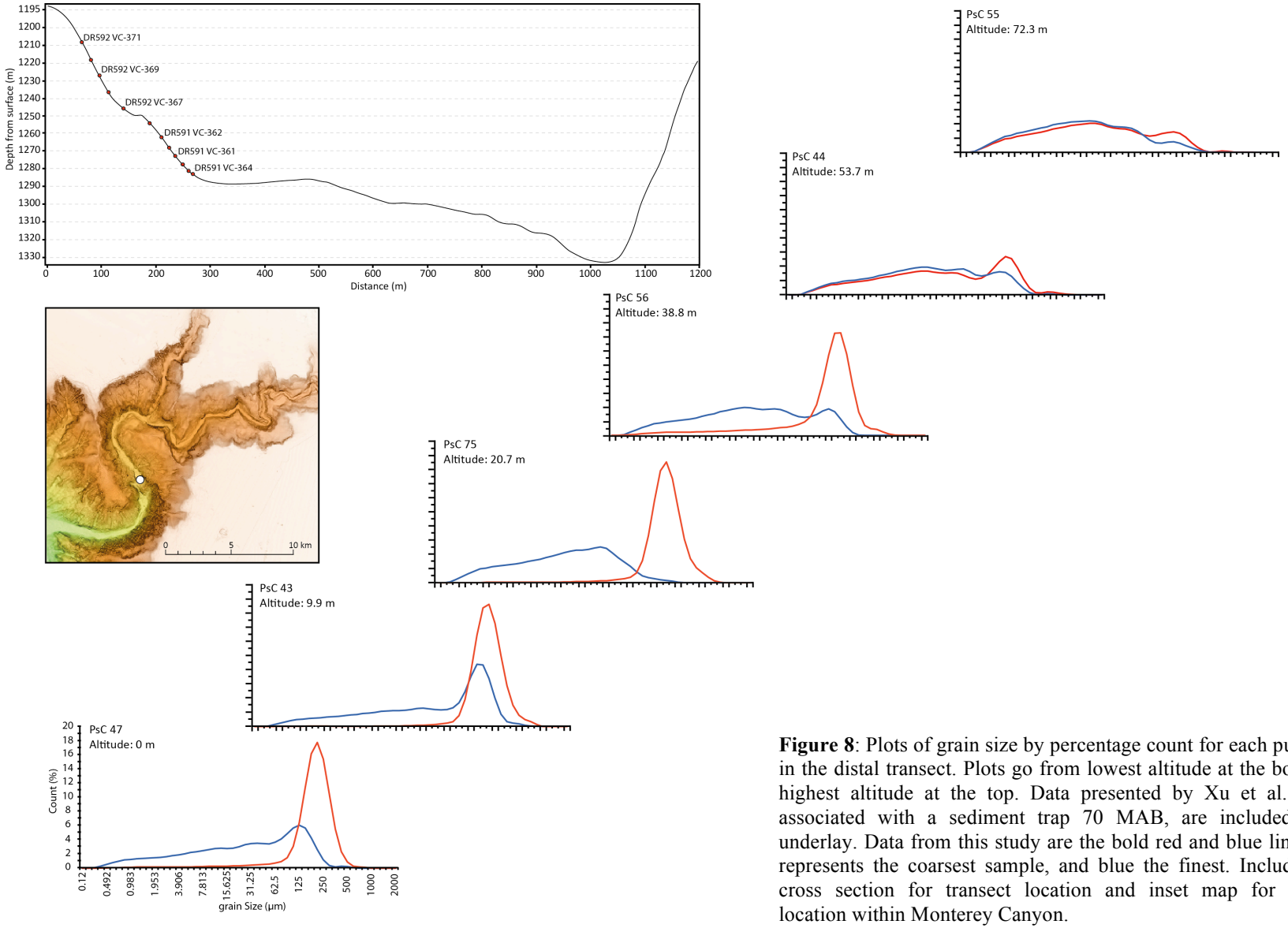

Figure 8: Plots of grain size by percentage count for each push core in the distal transect. Plots go from lowest altitude at the bottom to highest altitude at the top. Data presented by Xu et al. (2014) associated with a sediment trap 70 MAB, are included as an underlay. Data from this study are the bold red and blue lines. Red represents the coarsest sample, and blue the finest. Included is a cross section for transect location and inset map for transect location within Monterey Canyon.

trap at the same level. Push core 74 at 22 m altitude displays the most similar trends those presented by Xu et al (2014). A sharp peak of coarser material is seen, centr slightly finer than 250 μm, with a broader peak representing finer material. Same siz sand is therefore not found at ~70 m altitude on the canyon walls but is found at 22 altitude.

Sediment trap data from Xu et al's (2014) second location (our confluen transect) follows the same trend as their previous. A sharp, fining upwards peak centr around 62.5 μm is coupled with a broader dome beginning at 0.35 μm and extending 210 μm (figure 7). The amount of sand in this sediment trap is much higher than the fi sediment trap with only four measurements not being within sand. Push core 62 is at ~ m altitude and is the closest to the sediment trap altitude (70 M AB). Our samples do n show a sharp peak, representing a sand event, but do crosscut the peak of Xu et al (201 in a broad peak with a sharp drop off at the coarsest fraction (figure 7). The fine samp reaches a maximum of 300 μm, with the coarse sample having grains of 1000 μ detected. Both samples began at 0.35 μm. The lack of sharp peak but presence of grai of the size detected by Xu et al (2014) suggests that our samples are not a distinct sa event but are discrete grains of sand within a predominantly fine sample. We nevertheless see grains of the same size as those presented by Xu et al (2014). A distin peak representing an event, with the same size grains as Xu et al (2014) is seen in pu core 52 at an altitude of 48.6 m.

Unfortunately, data from a sediment trap at the distal transect were not availab and as such, only data from this study are presented (figure 8). By examining results fro push core 55 at 72 m altitude (the altitude most similar to previous sediment trap height the trends shown are most comparable to those at the proximal transect (figure 8) where broad peak is characteristic. The samples reach a maximum grain size of 500 μm, havi a finer limited of 0.35 μm. At an altitude of 39 m (push core 56), a clear event signatu with a sharp peak is seen, most similar to previous data presented by Xu et al (2014).

4.0 DISCUSSION

4.1 WHAT DO THE FACIES REVEAL ABOUT FLOW PROCESSES?

Four main facies are identified within the cores that were graphically logged from three transects. The position of these facies within a given transect and any structures that they contain give insight into possible formative mechanisms. Each facies will be considered in turn and inferences deduced about formative mechanisms.

Silt and mud is the most widespread facies present in the cores. Two clear sub-facies can be deduced based primarily on colour. Darker mud, typically dark grey and brown, is the most prevalent. A paler mud is consistently found above *normally graded sand*. Thus it is inferred that the paler mud is turbidite mud and the darker mud is probably hemipelagi in origin. It should also be noted that not all normally graded sands posses a turbidite mud cap.

Sand beds with clasts of cohesive mud is a facies associated with a transition in altitude between dominantly *chaotic sands* to *silt and mud* dominance. The mud is relatively firm and occurs in discontinuous irregular shaped patches with sharp edges that show low degrees of rounding, thus it is inferred that they are clasts. Within core DR591 VC-362 at depths of 44-50 cm individual mud clasts occur that contain laminations of fine silt. These laminations are not horizontal, suggesting that the mud that contained silt laminations has been transported from its position of deposition. Previous studies have inferred that similar firm mud clasts were derived from the canyon walls (Paull et al. 2005). The sand with irregular, cohesive mud facies is found between 20 and 30 m altitude above the thalweg, on, or just above terraces on the flanks of the canyon. This facies may resultant from small scale slumping of the canyon walls, which is prevalent in Monterey Canyon (Smith et al. 2005). The periodic failing of the canyon wall results in the transport of the *silt and mud facies* that disaggregate to form smaller mud clasts that become incorporated into sand beds.

Normally graded sands are the most widely distributed facies in altitude after *silt and mud*. These beds range in thickness between 0.5 to 10 cm but typically 1-2 cm. They occasionally contain sedimentary structures such as fine laminations, which combined with the normal grading suggest deposition from turbidity currents. *Normally graded sands* occur between altitudes of 20 m and 56 m in the proximal transect and between 4

m and 72 m in the confluence and distal transects. This implies that some flows are at least the thickness of the transect altitude (~ 72m) in the confluence and distal transects. The intermittent occurrence of these normally graded sands suggests that transport events are sporadic. However, a lack of age constraints means that recurrence intervals of these events remains unknown.

Chaotic sands are between 2 cm and 30 cm thick and typically are the only facies present within cores from the channel axis. In addition to this, the lack of general structure in the sand and the presence of large cobbles (up to 7 cm in the longest dimension) suggests rapid deposition from high-energy gravity flow events (Paull et al. 2005). The *chaotic sands* are restricted to less than 7 m altitude (from the thalweg). This is however an estimate as we do have continuous sampling of the canyon flanks, with the minimum vertical distance between two adjacent cores being 0.38 m and the maximum being 12.04 m. Nevertheless, without having these chaotic sands above at least 7 m suggests that high-energy conditions are restricted to the axial channel of Monterey Canyon. The typical grain size of the matrix within these thalweg deposits is 250 μm to 500 μm. Grain size of beach sand within Monterey Bay is of similar size and composition to these canyon sands. Thus we concur with the previous suggestion (e.g. Paull et al. 2005; Paull et al. 2010), that these channel axis deposits are derived from the beaches near the head of the canyon. It is thought that the beach sand is transported to the head of the canyon via longshore drift, temporarily deposited and subsequently flushed into the canyon (Paull et al. 2010).

4.2 ARE THE SAME GRAIN SIZES FOUND IN THE SEDIMENT TRAPS AND AT THE SAME HEIGHTS ON THE CANYON WALLS?

Systematic grain sizing of the push cores, which represent the uppermost ~20 cm of the canyon wall deposits enables direct comparison with the grain size data presented in Xu et al. (2014). By directly comparing the grain sizes from the sediment traps with the grain sizes present at different heights up the canyon walls, we can find at what altitude above the thalweg similar grain sizes are found, giving direct insights into the flows that deposited the grains.

It is important to note that not all of the sediment found in the traps necessarily came from turbidity currents. Some of the fine-grained sediment may be hemipelagic sediment that entered the trap in between turbidity current events. The sharp 250 μm peak presented by Xu et al. (2014), at the most proximal location represents turbidite sand. Broader peaks that represent silt and mud are present in minor amounts at the base of the sediment tube; the origin of this sediment is equivocal. This fine-grained material in the sediment trap has a very similar distribution to the sediments that we found on the side of the canyon at the same height; however, we do not find the coarse-grained peak in sediments from the canyon wall. Comparing our grain-size distribution to that of Xu et al. (2014) indicates that at an ~70 m altitude, the canyon wall deposits do not contain the sand-sized grains found in the sediment trap, therefore the deposits are not a good representation of the flow at the proximal transect location. The sharp peak of 250 um sand along with the broader distribution of mud and silt that Xu et al. (2014) present are found on the flanks of the canyon. 22 m altitude Grains of the same size as the sediment trap are commonly found below 22 m altitude on the walls of the canyon. A trace of sand-sized grains are found at 35 m altitude but this is a minor amount and are finer than the deposit of Xu et al. (2014).

At the confluence transect Xu et al. (2014) found a sharp peak centred on xxx um and a broader peak of silt and mud; thus the sand peak is a finer grain size in contrast to the more proximal sediment trap and comprises the majority of the deposit. Mud only constitutes the lowest 10 cm of the sediment tube. The canyon wall deposits show a broad peak from x um to x um, thus the deposits contain the same size range of sediment as was found in the sediment trap but the distribution is different because we do not find the peak at xxx um. Instead of a sand bed we are finding occasional grains of sand within a muddy matrix. Thus the deposits show evidence that a flow has travelled past the location and was voluminous enough to reach the altitude of both the sediment trap and the highest altitude core location (65 m). However, the velocity of the flow was sufficient to suspend the sediment load and therefore only ‘pebble-dashed’ the canyon walls with sand grains, rather than depositing a bed of sand. A grain-size distribution more similar to Xu et al. (2014), is found at an altitude to 15.4 m above the thalweg albeit the sand peak on the canyon walls is coarser than was found in the sediment trap. Interestingly, our fine

sample has a larger range of grain sizes, typically up to 500 μm than Xu et al. (2014) and our fine samples from the proximal.

Whilst, The most distal transect does not have associated sediment trap data , the grain-size distribution on the canyon walls is most similar to the grain-size distribution on the walls at the confluence location, thus we infer that the 'pebble-dashing' process is also occurring at this location.

4.3 ARE THE PUSH CORES REPRESENTATIVE OF THE VIBRACORES?

For this study we assumed that the deposits in the push cores were similar in age to the deposits in the sediment traps, however, this is something we intend to better constrain in the future (see future work below). However, it is useful to consider whether these push core deposits are representative of the greater time period represented by the vibracores. By comparing the maximum grain sizes in both the push core and vibracore from the same altitudes we see that despite variations associated with collection methods, similar trends are seen. This suggests that the push cores are in fact representative of a greater time period. This said however, using the maximum grain size may give an unrepresentative view of the deposits as a whole because one coarse event may skew the results. Another approach is to study the grain size results from the push cores and the graphical logs of the vibracores. The grain size results for the proximal transect show no sand at ~70 m altitude, as does the graphical log for the equivalent vibracore, meaning the push core results are representative. Contrastingly, the confluence and distal highest altitude vibracores both show distinct sand beds yet the equivalent push core results show discrete grains not in distinct beds. The results by Xu et al. (2014) are therefore more comparable to the vibracore deposits, at these locations.

4.4 HOW WELL DO SEAFLOOR DEPOSITS REPRESENT THE FLOWS THAT CREATED THEM?

Understanding how well seafloor deposits represent the flows that created them is vital in marine geology as a large amount of our understanding into turbidity current processes comes from their deposits. Previously, it has been difficult to answer this question because we have not had flow data and deposit data from the same location.

The presence of a distinct sand event in the sediment trap deployed by Xu et al. (2014) at the proximal transect shows a flow of at least 70 m thickness passed through this location. Our results from the canyon flank suggest that the highest altitude a sand event is represented at is 22 m. There is a clear disparity between the two deposits, highlighting that reconstructing flow thicknesses from deposits may not be as robust as previously thought. Based on the cores alone we would not assume that a 70 m thick flow had passed this location. A similar, slightly less bleak view can be taken at the confluence and distal transects. By studying the vibracores we can infer that flows do in fact reach a 70 m altitude, accurately representing the thickness of the flow based on sediment trap data. If we only had the push core results however, the representation of a flow passing through would be more cryptic as distinct sand beds are not represented. The presence of sand grains does however suggest that a flow at least 70 m thick has passed through.

4.5 WHY IS SAND NOT PRESENT AT THE PROXIMAL LOCATION AT THE SAME HEIGHT AS THE SEDIMENT TRAP?

It is shown that sand reaches at least ~70 m altitude above the thalweg at the confluence and distal transect locations. Sand, contrastingly, is absent from the proximal transect above 22 m altitude, despite a flow being recorded as high as 70 MAB by a sediment trap (Xu et al. 2014). We suggest three possible reasons for this result. Firstly, this could be a result of flow structure and evolution. Secondly, we propose that the absence of sand at the proximal transect could be a result of flow 'sloshing'. Thirdly, previous studies have shown that flows can reach a state whereby the turbidity current is not erosive or depositional, thereby bypassing the system (Stevenson et al. 2013). Therefore, we suggest bypassing as a possible cause of no sand at the proximal transect.

It is known that turbidity currents can evolve downslope, becoming thicker (Xu et al. 2014). If for example a turbidity current was relatively narrow then the sediment trap could have been engulfed by the flow without the flow reaching the walls of the canyon at the same height, perhaps only coming into contact with the canyon sides at a lower altitude e.g. at 22 m where sand is seen on the canyon walls in the proximal transect. As the flow travelled further it may have entrainined more water and perhaps sediment, becoming thicker and more voluminous. As the flow passed the two more distal transects,

it could have been in a state whereby it was wide enough at 70 m altitude to reach the walls of the canyon. However, at these distal locations the flow at 70m altitude was not fully depositional it only left occasional grains on the side of the canyon

Much like terrestrial river systems, turbidity currents have to negotiate submarine channel features such as bends. The result of this is for turbidity currents to superelevate around the bend, occasionally over spilling (Lamb et al. 2008; Straub et al. 2008; Parsons et al. 2010). Following the bend the turbidity current would take time to return to its pre-bend motion. Thus the top of the flow may not have a constant thickness across the channel, but instead the flow may be 'sloshing around'. Superelevation would cause a run-up of the turbidity current to a higher altitude on one wall than it would have normally reached (in a straight channel). The proximal transect is on the northern flank of the canyon, immediately before a clockwise curving bend. The turbidity current may be superelevating up the southern wall, which is perhaps why we don't see sand at the same altitudes as the sediment trap on the northern wall.

Turbidity currents that are non-depositional must be either erosive or bypassing (Parker et al. 1986; Sequeiros et al. 2009; Stevenson et al. 2013). No evidence for erosion is seen on the canyon walls at the same altitude as the sediment trap (although without accurate age constraints this is hard to determine) and could therefore suggest a bypassing flow whereby there is net balance between erosion and deposition of zero. This bypassing hypothesis sits hand-in-hand with an evolving flow hypothesis as the flow is becoming more voluminous with the continued entrainment of underlying sediment.

It is recognised that the current data set is rather limited with only three transects. Each of the discussed hypotheses is not mutually exclusive and interplay of each could possibly be occurring. With this restricted data set it is difficult to come to any specific reasons as to why the sand distributed differently at the three transects.

5.0 CONCLUSIONS/RECOMMENDATIONS

As a result of difficulties in directly monitoring turbidity currents, seafloor deposits are often used to reconstruct the currents and understand sediment transport processes. To

understand how well deposits from within the axial channel and the walls of Monterey canyon reflect flows that deposited them, three core transects were graphically logged and grain sized to directly compare with flow data. We provide the first direct comparison of flow deposits and flow measurements.

Turbidity current deposits sampled directly by Xu et al. (2014) had distinct grain size trends, showing the presence of sand beds and mud beds. Sand distribution on the canyon wall varied in altitude between the three core transect. Sand grains of the same size as the sediment trap were found discretely at the confluence and distal transects at 70 m altitude, whilst the proximal transect had no evidence of sand above 56 m on the canyon wall. The lack of sand most proximal could be a result of an evolving flow where the flow is restricted in thickness laterally but not in the centre of the canyon at the proximal transect. The flow is captured within the sediment trap but does not reach the same altitude on the wall of the canyon. The flow becomes more voluminous downslope and reaches ~70 m altitude on the canyon wall at the following two transects. Alternatively the flow could be superelevating around bends and 'sloshing' from side to side, only reaching 70 m altitude on one side of the canyon; the opposite side to the core transect at the proximal location. Finally, a bypassing flow whereby the flow is neither depositional nor erosional could be occurring and not leaving a trace at the proximal transect.

In order to test the discussed hypotheses, the data set would need to be enlarged. By coring at the same canyon location but on the opposite wall, if possible, the deposits from a sloshing flow would be captured. An elevated deposit on one wall would be countered by lower altitude sand deposit on the opposite wall. Additionally transects from new locations would test whether the flow is evolving downslope. More proximal transects than the current proximal transect would allow us to see whether sand is absent from a 70 m altitude on the canyon wall or whether the current proximal transect is an anomaly. The most pressing matter however is establishing an age of the deposits. Currently we are unsure whether the sampled push cores are similar in age to the sediment trap deposits. Traditionally, ^{14}C dating of foraminifera is used for dating marine sediment but the lack of foraminifera in our deposits eliminates this method. ^{210}Pb dating has been suggested, as this will allow us to establish sediment accumulation rates over the past 100 to 150

years, accurately constraining an age for our most recent deposits and therefore the deposits more comparable to the sediment trap deposits.

6.0 ACKNOWLEDGEMENTS

I would firstly like to thank Charlie Paull for not only his invaluable insights in Monterey Canyon but also for providing the cores for the study and for future work. I would also like to thank Esther Sumner for her continuing support with the project and my PhD studies and also for the amount of time proof reading the sections for this report. My time spent at the USGS, Santa Cruz would not have been possible without the assistance of Ange Tan and her expertise on the Coulter counter, for which I am extremely grateful. Thanks must also go to Jingping Xu for allowing us to use his data from the sediment traps otherwise this project would have been very difficult.

This internship would not have been possible without the time and expertise and George and Linda and I thank you for that. It has been an incredible 10 weeks, and ones that I will not forget.

Finally, thank you to everyone at MBARI for making the work I am, and will continue to do possible. You have all been so welcoming to all of the interns. This would not have been possible if it were not for the Packard Foundation.

References:

Barley, B., 1999. Deepwater problems around the world. *Leading Edge*, 18, pp.488–494.

Carter, L. et al., 2009. Submarine cables and the oceans: Connecting the world. *UNEP-WCMC Biodiversity Series 31. ICPC/UNEP/UNEP-WCMC*, p.64 (pp).

Cattaneo, a. et al., 2012. Searching for the seafloor signature of the 21 May 2003 Boumerdès earthquake offshore central Algeria. *Natural Hazards and Earth System Science*, 12(7), pp.2159–2172.

Galy, V. et al., 2007. Efficient organic carbon burial in the Bengal fan sustained by the Himalayan erosional system. *Nature*, 450(7168), pp.407–10.

Goldfinger, C. et al., 2007. Rupture lengths and temporal history of significant earthquakes on the offshore and north coast segments of the Northern San Andreas

Fault based on turbidite stratigraphy. *Earth and Planetary Science Letters*, 254(1-2), pp.9–27.

Hsu, S. et al., 2008. Turbidity Currents , Submarine Landslides and the 2006 Pingtung Earthquake off SW Taiwan. *Terr. Atmos. OCean. Sci*, 19(6), pp.767–772.

Hughes Clarke, J.E. et al., 2012. The Squamish ProDelta : Monitoring Active Landslides and Turbidity Currents. In *Canadian Hydrographic Conference 2012*. pp. 1–15.

Khripounoff, A. et al., 2003. Direct observation of intense turbidity current activity in the Zaire submarine valley at 4000 m water depth. *Marine Geology*, 194(3-4), pp.151–158.

Lamb, M.P. et al., 2008. Evidence for superelevation, channel incision, and formation of cyclic steps by turbidity currents in Eel Canyon, California. *Geological Society of America Bulletin*, 120(3-4), pp.463–475.

Liu, J.T. et al., 2012. Cyclone-induced hyperpycnal turbidity currents in a submarine canyon. *Journal of Geophysical Research*, 117(C4), p.C04033.

Parker, G., Fukushima, Y. & Pantin, H.M., 1986. Self-accelerating turbidity currents. *Journal of Fluid Mechanics*, 171, pp.145–181.

Parsons, D.R. et al., 2010. Gravity-driven flow in a submarine channel bend: Direct field evidence of helical flow reversal. *Geology*, 38(12), pp.1063–1066.

Paull, C.K. et al., 2013. Anatomy of the La Jolla Submarine Canyon system; offshore southern California. *Marine Geology*, 335, pp.16–34.

Paull, C.K. et al., 2003. Caught in the act: the 20 December 2001 gravity flow event in Monterey Canyon. *Geo-Marine Letters*, 22(4), pp.227–232.

Paull, C.K. et al., 2011. High-resolution bathymetry of the axial channels within Monterey and Soquel submarine canyons , offshore central California. *Geosphere*, 7(5), pp.1077–1101.

Paull, C.K. et al., 2010. Origins of large crescent-shaped bedforms within the axial channel of Monterey Canyon, offshore California. *Geosphere*, 6(6), pp.755–774.

Paull, C.K. et al., 2005. Trail of sand in upper Monterey Canyon: Offshore California. *Geological Society of America Bulletin*, 117(9), p.1134.

Piper, D.J.W. et al., 1999. The sequence of events around the epicentre of the 1929 Grand Banks earthquake : initiation of debris flows and turbidity current inferred from sidescan sonar. *Sedimentology*, 46, pp.79–97.

Piper, D.J.W. & Savoye, B., 1993. Processes of late Quaternary turbidity current flow and deposition on the Var deep-sea fan, north-west Mediterranean Sea. *Sedimentology*, 40, pp.557–582.

Pirmez, C. & Imran, J., 2003. Reconstruction of turbidity currents in Amazon Channel. *Marine and Petroleum Geology*, 20(6-8), pp.823–849.

Puig, P. et al., 2003. Shelf-to-canyon sediment-transport processes on the Eel continental margin (northern California). *Marine Geology*, 193(1-2), pp.129–149.

Puig, P., Palanques, A. & Martín, J., 2014. Contemporary Sediment-Transport Processes in Submarine Canyons. *Annual review of marine science*, 6, pp.1–25.

Sequeiros, O.E. et al., 2009. Experimental study on self-accelerating turbidity currents. *Journal of Geophysical Research*, 114, pp.1–26.

Shepard, F.P., 1981. Submarine Canyons: Multiple Causes and Long-Time Persistence. *American Association of Petroleum Geologists Bulletin*, 5, pp.1062–1077.

Smith, D.P. et al., 2005. Semiannual patterns of erosion and deposition in upper Monterey Canyon from serial multibeam bathymetry. *Geological Society of America Bulletin*, 117(9), p.1123.

Stevenson, C.J. et al., 2013. The flows that left no trace: Very large-volume turbidity currents that bypassed sediment through submarine channels without eroding the sea floor. *Marine and Petroleum Geology*, 41, pp.186–205.

Straub, K.M. et al., 2008. Interactions between turbidity currents and topography in aggrading sinuous submarine channels: A laboratory study. *Geological Society of America Bulletin*, 120(3-4), pp.368–385.

Sumner, E.J. et al., 2013. Can turbidites be used to reconstruct a paleoearthquake record for the central Sumatran margin? *Geology*, 41(7), pp.763–766.

Talling, P.J. et al., 2012. Subaqueous sediment density flows: Depositional processes and deposit types. *Sedimentology*, 59(7), pp.1937–2003.

Talling, P.J., Paull, C.K. & Piper, D.J.W., 2013. How are subaqueous sediment density flows triggered, what is their internal structure and how does it evolve? Direct observations from monitoring of active flows. *Earth-Science Reviews*, 125, pp.244–287.

Twichell, D.C. & Roberts, D.G., 1982. Morphology , distribution , and development of submarine canyons on the United States Atlantic continental slope between Hudson arid Baltimore Canyons Morphology , distribution , and development of submarine canyons on the United States Atlantic continent. *Geology*, 10, pp.408–412.

Xu, J.P., 2011. Measuring currents in submarine canyons: Technological and scientific progress in the past 30 years. *Geosphere*, 7(4), pp.868–876.

Xu, J.P., 2010. Normalized velocity profiles of field-measured turbidity currents. *Geology*, 38(6), pp.563–566.

Xu, J.P., Noble, M. a. & Rosenfeld, L.K., 2004. In-situ measurements of velocity structure within turbidity currents. *Geophysical Research Letters*, 31(9), pp.1-4

Xu, J.P., Sequeiros, O.E. & Noble, M. a., 2014. Sediment concentrations, flow conditions, and downstream evolution of two turbidity currents, Monterey Canyon, USA. *Deep Sea Research Part I: Oceanographic Research Papers*, 89, pp.11–34.